Microglia Activation and Recruitment of Circulating Macrophages During Ischemic Experimental Branch Retinal Vein Occlusion

Andreas Ebneter, Despina Kokona, Nadia Schneider, and Martin S. Zinkernagel

Department of Ophthalmology and Department of Clinical Research, Inselspital, Bern University Hospital, University of Bern, Switzerland

Correspondence: Martin S. Zinkernagel, Department of Ophthalmology, Inselspital, CH-3010 Bern, Switzerland; martin.zinkernagel@insel.ch.

AE and DK contributed equally to the work presented here and should therefore be regarded as equivalent authors.

Submitted: August 6, 2016
Accepted: January 5, 2017

Citation: Ebneter A, Kokona D, Schneider N, Zinkernagel MS. Microglia activation and recruitment of circulating macrophages during ischemic experimental branch retinal vein occlusion. *Invest Ophthalmol Vis Sci*. 2017;58:944–953. DOI:10.1167/iovs.16-20474

Purpose. To characterize retinal microglia activation and macrophage recruitment in experimental branch retinal vein occlusion (BRVO).

Methods. Experimental BRVO was induced in Balb/c mice and histologic changes were studied. Tissue hypoxia was visualized using pimonidazole hydrochloride. Monocyte-derived retinal cells were quantified using histology and flow cytometry. To investigate the dynamics of invading blood-borne macrophages, chimera mice were generated using bone marrow grafts from Cx3cr1$^{(gfp/gfp)}$ mice to rescue lethally irradiated wild-type BALB/c mice. Longitudinal in vivo imaging was performed to monitor cell invasion. The levels of proinflammatory cytokines in the retina were quantified by quantitative real-time PCR.

Results. Histology showed disruption of tissue architecture and temporary swelling with marked hypoxia coinciding with increased VEGF-A and hypoxia inducible factor-1α (HIF-1α) expression and elevation of proinflammatory cytokines within 3 days after experimental BRVO, followed by thinning of the inner retinal layers at later time points. Proinflammatory cytokine levels were elevated. Activation of resident retinal microglia and recruitment of circulating macrophages in areas of hypoxic retina were evident early after the insult and peaked at day 7, remaining elevated for up to 28 days. Flow cytometry showed upregulation of CD68 and major histocompatibility complex class-II (MHC-II) expression at day 3, culminating at day 7.

Conclusions. Experimental BRVO causes hypoxia and breakdown of the inner blood–retina barrier, followed by activation of microglia and invasion of macrophages from the systemic circulation. Consequently, treatments targeting microglia activation or macrophage recruitment might potentially mitigate the sequelae and attenuate degenerative changes induced by retinal vein occlusion.

Keywords: retinal vein occlusion, macular edema, optical coherence tomography, laser, photocoagulation, mouse model

Retinal vein occlusion (RVO) is the most common vascular eye disease after diabetic retinopathy, and causes vision loss due to macular edema, ischemia, and retinal atrophy.[1] Macular edema is the main cause of visual impairment in patients with RVO. Besides the established role of vascular endothelial growth factor (VEGF) in the formation of macular edema, inflammation seems to play a major role in pathogenesis and chronification.[2,3]

Retinal vein occlusion causes tissue ischemia, and triggers an inflammatory cascade that leads to breakdown of the inner blood–retina barrier,[4] which involves adhesion molecules and a plethora of inflammatory mediators. Elevated vitreous[5–7] and aqueous humor[8] levels of presumably involved interleukins (IL-1β, IL-2, IL-5, IL-6, IL-8, IL-9, IL-10, IL-12, IL-13), chemokines (CCL11, CXCL10, CCL2, CCL4), granulocyte-colony stimulating factor (G-CSF), interferon-γ (IFN-γ), tumor necrosis factor (TNF), and VEGF have been identified in patients with RVO. Importantly, vitreous levels of mediators such as VEGF and IL-6 correlated independently with vascular permeability and the severity of macular edema.[9] Resident microglia are important contributors to inflammation after injury. However, invading macrophages presumably also help clear debris and restore tissue integrity.[10] Yet overactivation might be detrimental.[11]

Macrophages are a major source of many cytokines, such as TNF, IL-1, IL-6, IL-8, and IL-12, and central in the regulation of inflammatory processes.[12] As the inflammatory responses may be influenced at different stages of RVO by therapeutic agents such as intravitreal steroids[13,14] or anti-VEGF agents,[15–17] a better understanding of the cascade of inflammation following RVO may help guide treatment decisions.

While a wide body of knowledge exists on the role of macrophages in disease of the outer retina[18,19] and experimental data are available,[20] little is known about the dynamics of macrophages during RVO, a chronic disease of the inner retina characterized by hypoxia. We and others have previously described a mouse model of experimental branch retinal vein occlusion (BRVO).[21,22] Here, we aimed at gaining a better understanding of the contribution of macrophages on the

course of RVO using histology and fluorescence-activated cell sorting (FACS) of the retina.

Materials and Methods

Animals

This study was approved by the local Animal Ethics Committee (Veterinärdienst des Kantons Bern: BE 38/13) and conformed to the ARVO Statement for the Use of Animals in Ophthalmic and Vision Research. BALB/c AnNCrl mice (5–6 weeks old; Charles River Laboratories, Sulzfeld, Germany) and locally bred Cx3cr1$^{(gfp/gfp)}$ mice on a Balb/c background were used for this study. Animals were housed in groups of two to five under temperature- and humidity-controlled conditions in individually ventilated cages with a 12-hour light/12-hour dark cycle. Mice were anesthetized by intraperitoneal injection of 1 mg/kg medetomidine (Dormitor 1 mg/mL; Provet AG, Lyssach, Switzerland) and 80 mg/kg ketamine (Ketalar 50 mg/mL; Parke-Davis, Zurich, Switzerland) for laser procedures. Atipamezol (Antisedan 5 mg/mL; Provet AG) was used to antagonize medetomidine at the end of the intervention. Pupils were dilated with tropicamide 0,5%/phenylephrine 2.5% eye drops (Hospital Pharmacy, Inselspital, Bern, Switzerland). At the end of the experiment, mice were euthanized by carbon dioxide inhalation or by terminal anesthesia with pentobarbital (200 mg/kg body weight given intraperitoneally).

Overall, 245 eyes of 126 mice of either sex were included in this study. A total of 142 eyes were subjected to laser-induced BRVO, and 88 eyes were used as lasered controls (control). The remaining 22 eyes were from naïve animals. The BRVO eyes were analyzed as follows: 20 eyes for histology, immunohistochemistry, and in situ hybridization; 16 eyes for retinal whole mounts; 16 chimera eyes for fundus autofluorescence imaging (FAF); 6 eyes for the hypoxia marker staining; 60 eyes for FACS analysis; and 24 eyes for quantitative real-time polymerase chain reaction analysis (qRT-PCR). The controls (88 eyes) were evaluated as follows: 12 eyes for histology, immunohistochemistry, and in situ hybridization; 8 eyes for retinal whole mounts; 16 chimera eyes for FAF; 4 eyes for the hypoxia marker staining; 32 eyes for FACS analysis; and 16 eyes for qRT-PCR. The remaining 22 eyes were from naïve animals and were analyzed as follows: 2 eyes for retinal whole mounts, 12 eyes as naïve controls for FACS analysis, and 8 eyes for qRT-PCR. In total, seven eyes had to be excluded from the final analysis due to vitreous hemorrhages.

Laser-Induced Vein Occlusion

Branch retinal vein occlusion was induced by 532-nm laser photocoagulation (Visulas 532s; Carl Zeiss Meditec AG, Oberkochen, Germany) with a slit-lamp adapter (Iridex Corporation, Mountain View, CA, USA) mounted on a slit-lamp (BM900; Haag-Streit AG, Koeniz, Switzerland) as described elsewhere.[21] A small 2-mm fundus laser lens for mice (Ocular Instruments, Inc., Bellevue, WA, USA) was used to visualize the fundus and blood vessels during the laser application. Only one vein was targeted, and occlusion was considered complete when stasis of the blood flow distal from the laser burn was seen during direct fundus observation. In control mice, retinal laser burns of the same intensity (160 mW, 800 ms) were performed at comparable distance from the optic nerve but sparing retinal blood vessels.

Generation of Bone Marrow Chimeras

In total, eight recipient Balb/c AnNCrl mice were lethally irradiated with two doses of 6.0 Gy given 14 hours apart without shielding of the eyes. Three donor Cx3cr1$^{(gfp/gfp)}$ mice were euthanized, and their femurs and tibias were collected. The bone marrow was removed, and single-cell suspensions were generated in CSM buffer (2% fetal bovine serum [FBS], 1% penicillin-streptomycin, 0.01 M HEPES in Hanks' balanced salt solution). The cells were filtered through a 70-μm mesh filter followed by centrifugation at 18*g* for 5 minutes at 4°C. Pelleted cells were resuspended in Dulbecco's modified Eagle's medium (DMEM) medium (Thermo Fisher Scientific, Waltham, MA, USA) containing 2% FBS, and live cells were counted using trypan blue. Recipient irradiated mice received a single intravenous injection of 1 to 2 $\times$ 10^6 bone marrow cells within a maximum of 3 hours after the second dose of irradiation. Bone marrow chimera mice received antibiotics (0.8 mg/mL sulfamethoxazol and 0.16 mg/mL trimethoprim) provided in the drinking water for 2 weeks after the transplantation. One week after bone marrow transplantation, experimental BRVO was induced in chimera mice.

Fundus Autofluorescence Imaging

The presence and distribution of green fluorescent protein (GFP)-positive microglia/macrophages in the retina were longitudinally monitored for several weeks after experimental BRVO with blue light (488 nm) FAF. Fundus autofluorescence images were acquired at high resolution of 1536 $\times$ 1636 pixels using a noncontact ultra-widefield 102° lens (Heidelberg Engineering GmbH, Heidelberg, Germany).

Hypoxia Marker

Pimonidazole hydrochloride (Hypoxyprobe-1; Hypoxyprobe, Inc., Burlington, MA, USA) was intraperitoneally injected at a dosage of 60 mg/kg body weight in selected mice 90 minutes prior to killing the animals at day 1 and 4 after experimental BRVO. The harvested tissue was fixed and processed for paraffin embedding as detailed below for immunohistochemistry.

Histology

Retinal sections were stained with standard hematoxylin–eosin at different time points after BRVO. Briefly, the sections were deparaffinized, rehydrated, and consecutively stained with hematoxylin and eosin following standard protocols. The sections were then dehydrated and mounted with Eukitt (O. Kindler GmbH & Co, Freiburg, Germany).

Immunohistochemistry Studies

At selected time points after induction of BRVO, eyes from euthanized mice were removed and fixed in 4% paraformaldehyde (pH 7.4) for 24 hours. Before removal from the animal, the orientation of the eyes was marked by placing a suture at the limbus and ensuring correct orientation of specimens during embedding, since BRVO was systematically induced in the superonasal quadrant. Eyes underwent routine paraffin processing, and tissue sections of 5-μm thickness were cut with a microtome (Leica Biosystems, Muttenz, Switzerland) and collected on slides. Tissue sections were deparaffinized and rehydrated before antigen retrieval with Tris–EDTA buffer (pH 9.0), as previously described in more detail elsewhere.[23] A rabbit polyclonal antibody against ionized calcium-binding adapter molecule 1 (anti-Iba1 rabbit polyclonal antibody, Wako Cat. No. 019-19741; Wako Pure Chemical Industries Ltd., Osaka, Japan) was applied overnight as the primary antibody to mark microglia. Visualization was achieved by incubation with a secondary goat anti-rabbit IgG (H+L), Alexa Fluor 594

conjugate (1:1000, A27016; Thermo Fisher Scientific. To stain Müller cells, an anticellular retinaldehyde-binding protein rabbit antibody (sc-28193; 1:300; Santa Cruz Biotechnology, Inc., Dallas, TX, USA) was used as primary antibody, followed by the secondary goat anti-rabbit antibody (see above). Slides were mounted with mounting medium containing 4′,6-diamidino-2-phenylindole (DAPI) (Vector Laboratories, Burlingame, CA, USA), coverslipped, and examined under the microscope.

Immunohistochemical staining of protein adducts of pimonidazole in hypoxic cells was achieved using a 1:50 dilution of an anti-pimonidazole mouse IgG1 monoclonal antibody (hybridoma clone 4.3.11.3, Lot 9.7.11; Hypoxyprobe, Inc.) as the primary antibody overnight, followed by a goat anti-mouse IgG (H+L) secondary antibody (Alexa Fluor 488 conjugate; 1:250, A11001; Thermo Fisher Scientific).

For preparation of retinal whole mounts, eyes were removed and fixed in 4% paraformaldehyde solution (pH 7.4) for 10 minutes. The anterior segment was removed, and the posterior portion, including the retina, was incubated for another 50 minutes in 4% paraformaldehyde (pH 7.4). Fixed retinas were mechanically detached from the choroid and extensively washed in 0.1% Triton in PBS followed by incubation in 5% normal goat serum (NGS) in 0.1% Triton in PBS for 2 hours at room temperature. Isolectin GS-IB4 from *Griffonia simplicifolia* (Alexa Fluor 647 conjugate; 1:100 in 5% NGS in 0.1% Triton in PBS; Thermo Fisher Scientific) and the rabbit polyclonal antibody against Iba-1 (see above) were used for double labeling of blood vessels and microglia cells, respectively. Retinas were incubated with primary antibodies for 48 hours at 4°C. A secondary goat anti-rabbit IgG (H+L) (Alexa Fluor 594 conjugate; 1:1000, A27016; Thermo Fisher Scientific) was used for the visualization of Iba-1 staining. In the chimera mice, a chicken polyclonal antibody against GFP (1:100, ab13970; Abcam, Cambridge, UK) was used for labeling of bone marrow–derived macrophages, followed by incubation with a preabsorbed goat polyclonal antibody to chicken IgY H+L (FITCH) (1:1000, ab7114; Abcam). Retinas were extensively washed in PBS–0.1% Triton, four radial cuts were made, and the retinas were flat mounted on a slide with the ganglion cell layer facing up. Whole mounts were coverslipped and examined under a confocal microscope.

Microscopy

Retinal sections were examined under an epifluorescence microscope (Olympus BX60 microscope; Olympus, Tokyo, Japan). Photoshop (Version 7.0; Adobe Systems, San Jose, CA, USA) was used to adjust light and contrast. Retinal whole mounts were imaged using an inverted Zeiss LSM 710 fluorescence confocal microscope (Carl Zeiss Meditec AG). Z-stacks of 59.6 ± 4.6 μm of tissue (mean ± SEM) with 1-μm interval were obtained and finalized with the Imaris software (Version 7.1; Bitplane AG, Zurich, Switzerland). All figures were prepared using CorelDraw (Corel Corporation, Ottawa, ON, Canada).

Fluorescence-Activated Cell Sorting

Retinas from experimental mice were dissected at different time points after BRVO induction and processed for FACS analysis. The two retinas from the same mouse were combined to one sample. Briefly, the retinas were dissociated in 0.4 Wünsch Liberase TM Grade (Roche, Basel, Switzerland) in Dulbecco's phosphate-buffered saline (DPBS) at 37°C for 30 minutes. Single-cell suspensions were obtained and stained with DAPI (Thermo Fisher Scientific) for detection of dead cells.[24] The samples were washed in DPBS and resuspended in FACS buffer (100 mM EDTA, 20% FBS, 0.5% Na azide, in DPBS) for antibody staining; DNase I (0.01%, (Roche) was present in all solutions. Macrophages were identified using fluorescent-labeled antibodies against CD45 (30-F11, No. 103116, 1:100), CD11b (M1/70, No. 101212, 1:100), MHC-II (major histocompatibility complex class-II, AF6-120.1, No. 116422, 1:100), and CD68 (FA-11, No. 137010, 1:100) from Biolegend (San Diego, CA, USA). Samples were incubated for 20 minutes with antibodies and then analyzed with a LSR II Cytometer System using the BD FACSDIVA software (BD Biosciences, Allschwil, Switzerland). Analysis of the FACS data was performed in the Flowjo Single Cell Analysis Software V10 (TreeStar, Ashland, OR, USA).

In Situ Hybridization Studies

Customized probes (Cat. No. 312931, Accession No. NM_001025257.3; Advanced Cell Diagnostics SRL, Vignate, Italy) to detect mRNA for VEGF-A were used for in situ hybridization using the RNAscope 2.0 Red FFPE Kit (Cat No. 310036; Advanced Cell Diagnostics SRL) and an automated platform (Discovery Ultra; Ventana Medical System–Roche, Tucson, AZ, USA). The probe region covers 3106 bp spanning nucleotides 124 to 3230. Expression of dihydrodipicolinate reductase (DapB) mRNA from *Bacillus subtilis* and ubiquitin C (UBC) mRNA were used as negative and positive controls, respectively. Tissues were examined with bright-field microscopy at ×40 magnification, and the signal was semiquantitatively assessed.

Quantitative Real-Time PCR

Total RNA was isolated using the RNeasy Micro Kit (Qiagen, Hombrechtikon, Switzerland) per the manufacturer's instructions. Total RNA concentration was measured with a spectrophotometer (Nanodrop 1000; Thermo Fisher Scientific), and cDNA was synthesized from 1 μg total RNA using the iScript cDNA Synthesis Kit (Bio-Rad, Hercules, CA, USA) according to the manufacturer's instructions. The qRT-PCR reaction mix was prepared to a final volume of 10 μL and included 6 μL 1× iTaq Universal SYBR Green Supermix (Bio-Rad), 1 μL of each forward and reverse primer, and 2 μL 100 ng cDNA. The qRT-PCR was performed using an iQ5 real-time PCR Detection System (Bio-Rad). The following primer pairs were used:

b-actin: forward 5′-GCTGAGAGGGAAATCGTGCGTG-3′
reverse 5′-CAGGGAGGAAGAGGATGCGG-3′
VEGF-A: forward 5′-CAGGCTGCTGTAACGATGAA-3′
reverse 5′-TATGTGCTGGCTTTGGTGAG-3′
TNF-α: forward 5′-TGTTCATCCATTCTCTACCCAGCCC-3′
reverse 5′-GTCACTGTCCCAGCATCTTGTGTTT-3′
IFN-γ: forward 5′-GCCTCACCGCCTATCACTCC-3′
reverse 5′-GGGTCGTGCTCTGCCATCTT-3′
HIF1-α: forward 5′-TCATCAGTTGCCACTTCCCCAC-3′
reverse 5′-CCGTCATCTGTTAGCACCATCAC-3′

Quantitative RT-PCR reactions were carried out in duplicate, and only comparative threshold cycle (Ct) values leading to a Ct mean with a standard deviation below 0.1 were considered. To assess the presence of primer–dimers and to check for potential contamination, a negative control was included on each plate. Primer efficiencies were checked, and only primers with efficiencies between 90% and 110% were used. The ΔCt method was used to calculate relative gene expression levels with β-actin as a housekeeping gene for normalization of gene expression levels. Two retinas from the same mouse were used as one sample. Results were standardized relative to levels measured in naïve retinas.

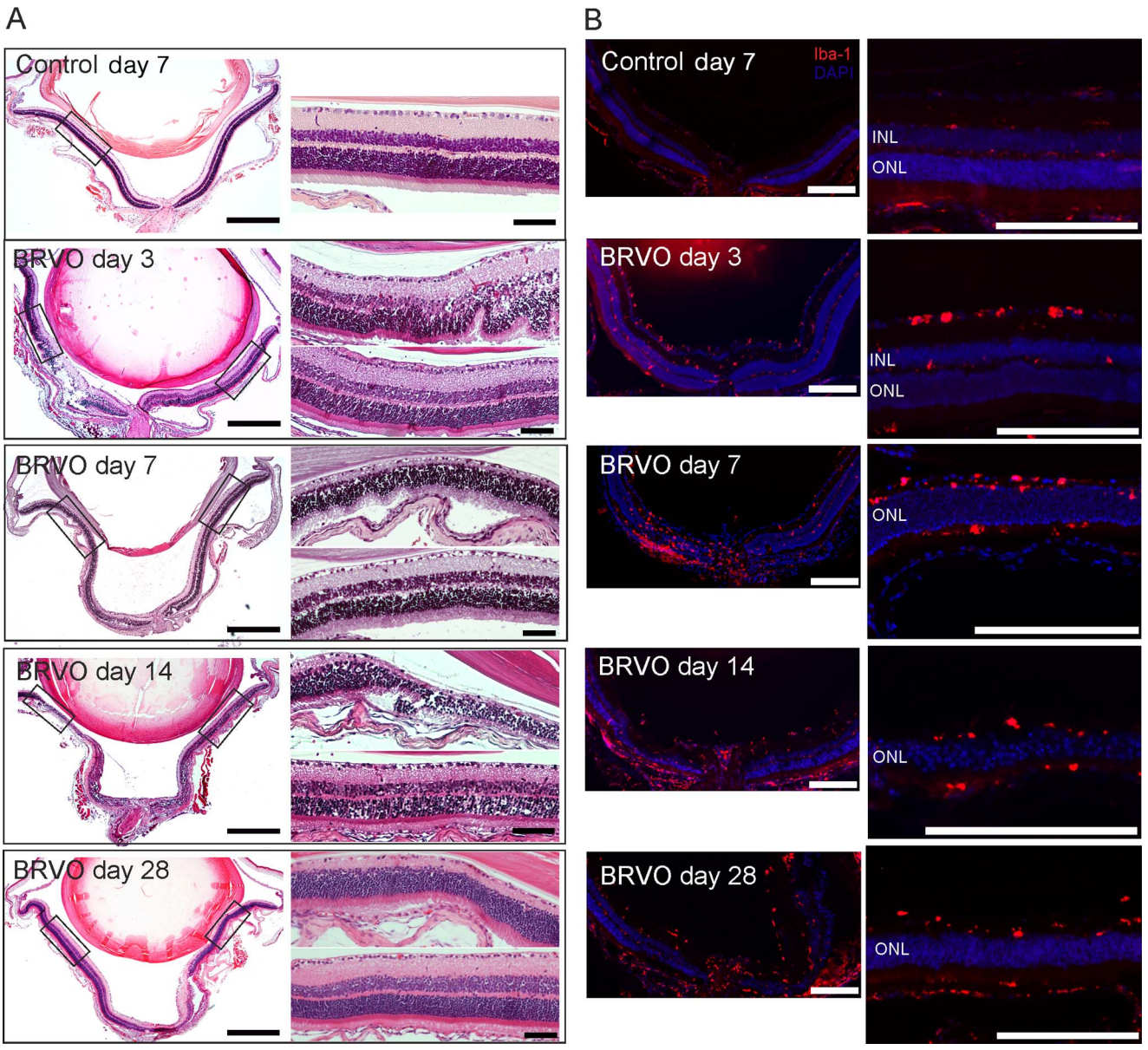

Figure 1. Retinal morphology and microglia activation in experimental BRVO. (**A**) Representative images of hematoxylin–eosin staining in control ($n = 3$ at each time point) and BRVO-subjected retinas 3, 7, 14, and 28 days after the laser application ($n = 5$ at each time point). Transient retinal swelling was observed in the area of the laser lesion 3 days after treatment. Formation of retinal folds at the laser site was also commonly found; however, postmortem artifacts from processing cannot be excluded. At days 7, 14, and 28, the inner retinal layers were thinned in the areas of the retina affected by vein occlusion (*upper right images*). In unaffected areas of the retina, the normal morphology was preserved (*lower right images*). *Scale bars*: 500 µm (*left microphotographs*); 50 µm (*right microphotographs*). (**B**) Representative images of Iba-1 immunoreactivity in control and BRVO-subjected retinas. Increased numbers of Iba-1–positive cells were present globally in BRVO retinas. The highest density was noted in areas affected by hypoxia (*images on the right*) and at the laser site (day 7, *on the left*). *Scale bars*: 100 µm (*left images*); 200 µm (*right images*). INL, inner nuclear layer; ONL, outer nuclear layer. No changes were seen in the control retinas (laser burn of identical intensity but not involving a retinal vein) at the different time points. Thus, only representative pictures of control retinas at day 7 are presented in (**A**, **B**), respectively.

Statistics

GraphPad Prism 5.0 software (GraphPad Software, Inc., San Diego, CA, USA) was used for the statistical analysis. Statistically significant differences of the qRT-PCR data were determined using 2-way ANOVA with Bonferroni correction for post hoc tests. One-way ANOVA followed by post hoc tests with Tukey's correction was used for the analysis of differences in the FACS data. *P* values less than 0.05 were considered statistically significant. All data are expressed as mean ± SEM.

Results

Histologic Changes

The histologic analysis of hematoxylin–eosin sections (Fig. 1A) showed disruption of the tissue architecture and transient swelling of the retina in the area of the laser lesions, sometimes with formation of retinal folds at early time points. After 7 days, there was obvious thinning of the inner layers of the retina in regions distally to the vein occlusion site (Fig. 1A, upper right images). The morphology in unaffected areas of retina was unaltered (Fig. 1A, bottom right images). Analysis of retinal

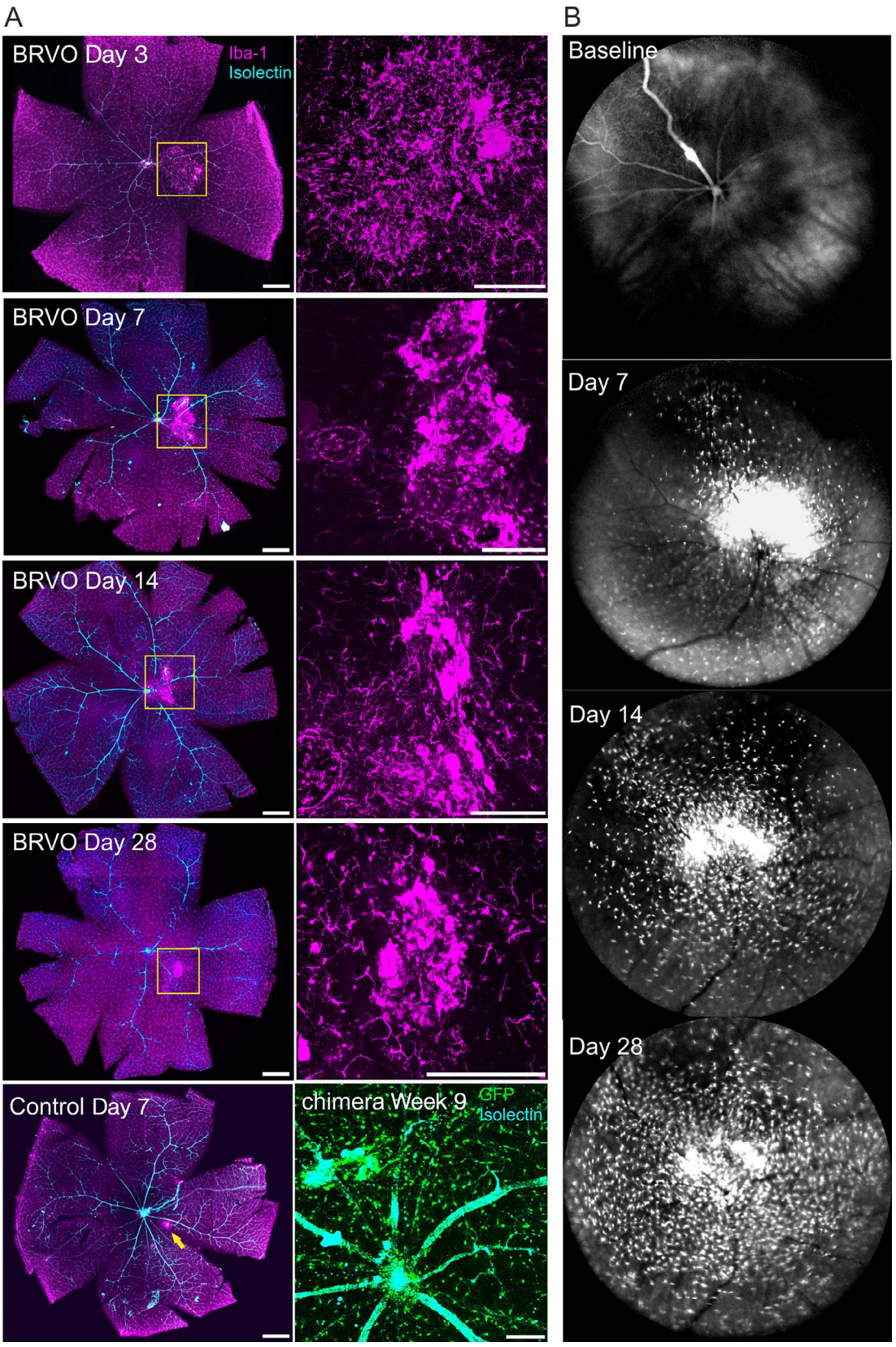

Figure 2. Macrophage invasion in retinas with experimental BRVO. (**A**) Retinal whole mounts at different time points after BRVO ($n = 3$ at each time point) and control retina ($n = 2$ for each time point) stained for Iba-1. The blood vessel endothelium is labeled with isolectin B4. In the BRVO retinas, Iba-1–positive cells are accumulating at the laser site (*yellow boxes*, *magnified on the right*). No changes were observed in control retinas at the different time points (laser burn of identical intensity away from retinal vein; representative picture of a control retina at day 7 shown; the *yellow arrow* indicates the site of the laser burn). Representative retinal whole mount of a chimera mouse 9 weeks after experimental BRVO, corresponding to 10 weeks after bone marrow transplantation, is depicted in the *bottom right image* (chimera). GFP-positive circulating

Investigative Ophthalmology & Visual Science

macrophages have invaded the laser site (*upper left corner*) and the retina. *Scale bars*: 500 μm (*left images*); 200 μm (*right images*), 500 μm (chimera). (**B**) Longitudinal analysis of macrophage invasion in representative Cx3cr1 bone marrow chimera mouse after experimental BRVO. Accumulation of macrophages at the laser site is evident 7 days after the insult with lightly scattered macrophages in the rest of the retina. At days 14 and 28, macrophage density is clearly increased in the peripheral retina too. The baseline picture was taken immediately after laser application to the vein in the left superior quadrant. The bright fluorescence in this vein originates from the rose bengal dye trapped in the occluded vessel and the thrombus (dilated portion close to the optic nerve head), whereas in the other blood vessels the rose bengal has been washed out.

cross sections stained for Iba-1 at various time points after induction of BRVO showed markedly increased numbers of Iba-1–positive cells at the site of laser lesion, peaking at day 7 (Fig. 1B). Moreover, there was an increase in the number of Iba-1–positive cells distal to the sites of vein occlusion. Retinal whole mounts (Fig. 2A) revealed that, compared to controls, the density of Iba-1–positive cells was increased not only in areas of ischemia or direct laser damage, but also in areas of the retina not directly affected by the experimental intervention. In the whole mounts of BRVO eyes, Iba-1–positive microglia/macrophages were primarily detected in the inner and outer plexiform layers in confocal microscopy. In areas with significant infiltration of macrophages (optic nerve, laser site), the morphology was more commonly of the amoeboid type, suggesting blood-derived macrophages, whereas in other parts of the retina the cells had a more ramified appearance. Whole mounts were additionally stained with isolectin B4 to better illustrate the relationship of Iba-1–staining cells with retinal blood vessels. Infiltrating macrophages and microglia densely lined the walls of the blood vessels damaged by the laser burn. This pattern was also discernible when evaluating macrophage invasion in chimeras.

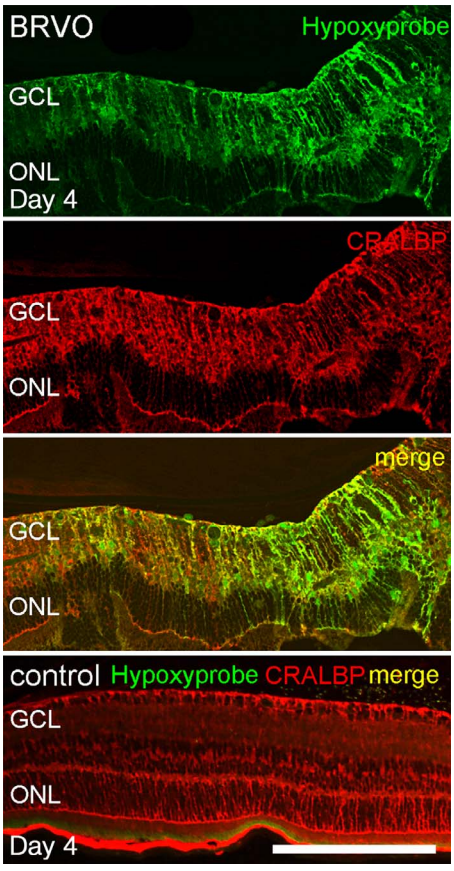

Figure 3. Double labeling of BRVO-affected retina with hypoxia marker. A representative retinal cross section from an animal euthanized 4 days after experimental BRVO is shown with ischemic portions toward the right of the images. A hypoxia marker (hypoxyprobe [*green*]) is predominantly found in Müller cells, labeled with anticellular retinaldehyde-binding protein antibody (CRALBP [*red*]). A retinal section of a control animal stained similarly is shown in the *bottom picture*. *Scale bar*: 200 μm. GCL, ganglion cell layer; ONL, outer nuclear layer.

Longitudinal In Vivo Analysis Using FAF in Cx3cr1 Bone Marrow Chimera Mice

Fundus autofluorescence imaging at different time points after BRVO induction (Fig. 2B) revealed invasion of circulating macrophages into the retina and accumulation around the laser site, which peaked 7 days after experimental BRVO. At this early time point, macrophages were clustering around the laser site with only scattered cells in the periphery. Twenty-eight days after the insult, invading macrophages were more homogeneously distributed over the retina but still at higher density in the supply territory of the occluded retinal vein. At the end of the experiment, the invading macrophages in whole mounts were analyzed by confocal microscopy after enhancing the GFP signal by immunolabeling. In the inner retinal layers, amoeboid GFP-positive cells were detected, while in deeper layers, most of the GFP-positive cells had a more ramified morphology, typical of resting microglia (Supplementary Fig. SC).

Double Labeling With Hypoxia Marker

Retinal cross sections from selected animals injected with pimonidazole hydrochloride ante mortem revealed extensive areas of hypoxia after experimental vein occlusion (Fig. 3). The morphology suggested that protein adducts of reductively activated pimonidazole were mainly localized in Müller cells, which was confirmed by double labeling sections for cellular retinaldehyde-binding protein.

Quantification of Macrophage Accumulation With FACS

At different time points after the laser application, FACS was performed in naïve and BRVO-subjected retinas (Fig. 4). $CD45^+CD11b^+$ cell populations, most probably representing primarily macrophages, were elevated 3, 7, and 14 days after BRVO, and then returned to control levels 28 days post BRVO (Fig. 4A). For quantification of the activated macrophage population (Fig. 4B), we examined the number of major histocompatibility complex class II (MHC-II)- and CD68-positive cells. The number of $CD45^+CD11b^+CD68^+$ cells was significantly elevated at all time points, while the number of $CD45^+CD11b^+CD68^+MHC\text{-}II^+$ cells was significantly elevated at all but the last time point (day 28). Macrophage activation peaked 7 days after BRVO and steadily decreased over time.

In Situ Hybridization of VEGF mRNA in the BRVO Retinas

In situ hybridization was performed in control and BRVO retinas 3 and 7 days after the laser application for qualitative assessment of VEGF mRNA levels in the retina. Levels of VEGF

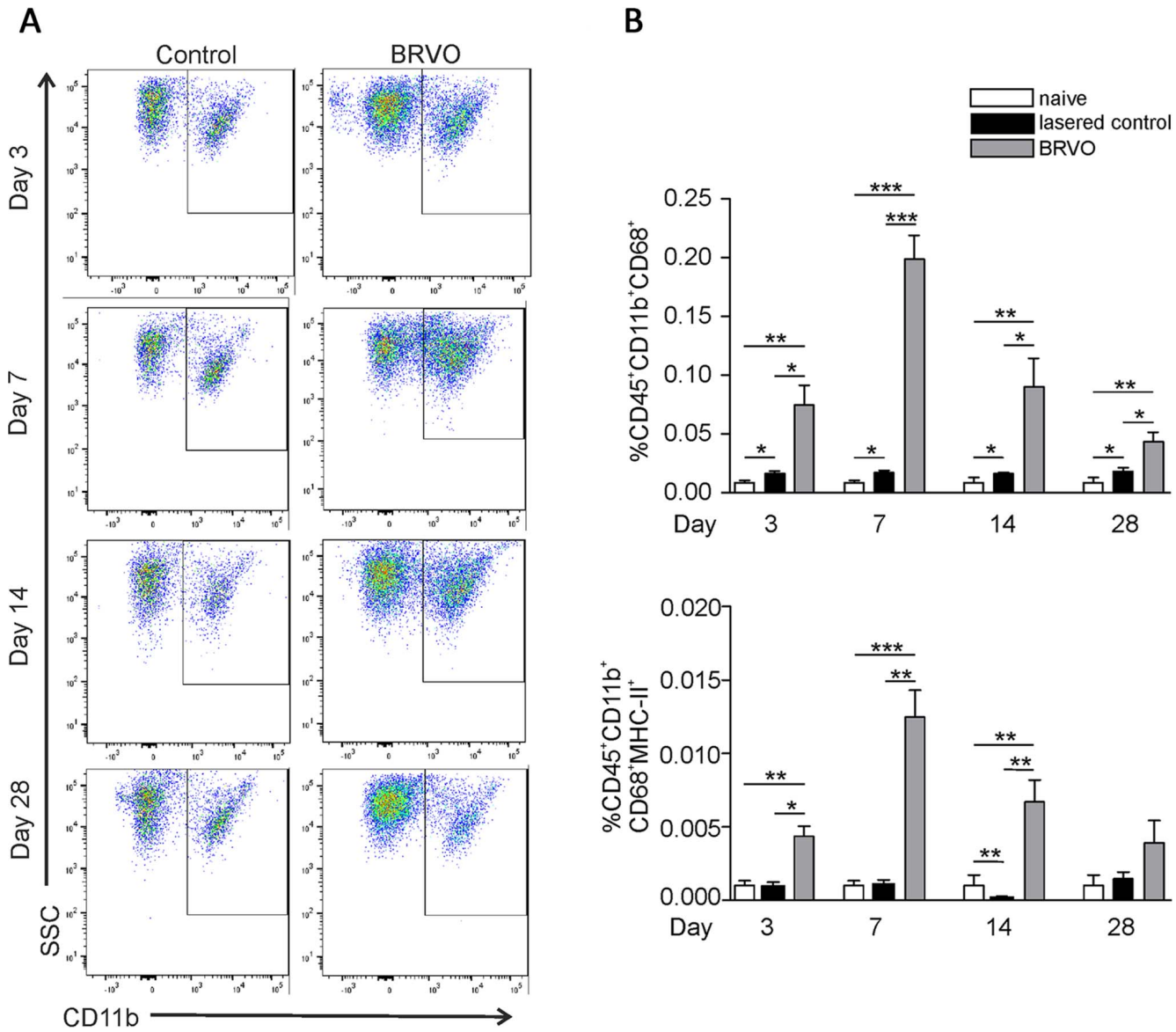

FIGURE 4. Macrophage dynamics in experimental BRVO–FACS analysis. (**A**) Representative FACS plots at different time points after the insult quantifying $CD45^+CD11b^+$ cells (*top right boxes*). The population of $CD45^+CD11b^+$ cells is increased in retinas after experimental BRVO. (**B**) Quantification of phagocytic macrophage population ($CD45^+CD11b^+CD68^+$) and the portion expressing MHC class II molecules ($CD45^+CD11b^+CD68^+MHC\text{-}II^+$). Macrophage accumulation peaked 7 days after experimental BRVO ($^*P < 0.05$, $^{**}P < 0.01$, $^{***}P < 0.001$; 1-way ANOVA with Tukey post hoc test). Naïve (without any laser): $n = 6$; controls (laser burn of identical intensity away from retinal vein): $n = 4$ each time point; BRVO: $n = 6$ for days 3 and 7, $n = 9$ for days 14 and 28.

mRNA were elevated compared to controls on days 3 and 7 after experimental BRVO. At both time points, VEGF mRNA was primarily detected in the inner nuclear layer (Fig. 5A). Later time points were not examined.

PCR of Hypoxia Markers and Inflammatory Cytokines in the Retina After BRVO

For relative quantification of hypoxia and proinflammatory cytokines, qRT-PCR was performed (Fig. 5B). Levels of VEGF-A mRNA were not altered at any of the time points examined. In contrast, HIF-1α mRNA expression was increased 3 and 7 days after BRVO ($^*P < 0.05$ and $^{**}P < 0.01$ compared to control). Relative quantification of proinflammatory cytokines revealed elevation of IFN-γ mRNA at day 3 ($^*P < 0.05$), while at day 7, IFN-γ levels were not different from control retinas. The mRNA levels of other proinflammatory cytokines examined (data not shown) did not show any statistically significant change during the first week. On days 14 and 28 after BRVO, none of the markers analyzed were elevated compared to controls.

DISCUSSION

Retinal vein occlusion supposedly has many similarities with an ischemic stroke, since the neuroretina forms part of the central nervous system. Inflammatory processes determine the pathophysiology after the hypoxic insult in the central nervous system, and modulation of inflammation can influence the sequelae of an ischemic event.[25]

Here, we showed that the presence of activated microglia and invading macrophages in the retina is pronounced after experimental RVO. These cells play a central role in the

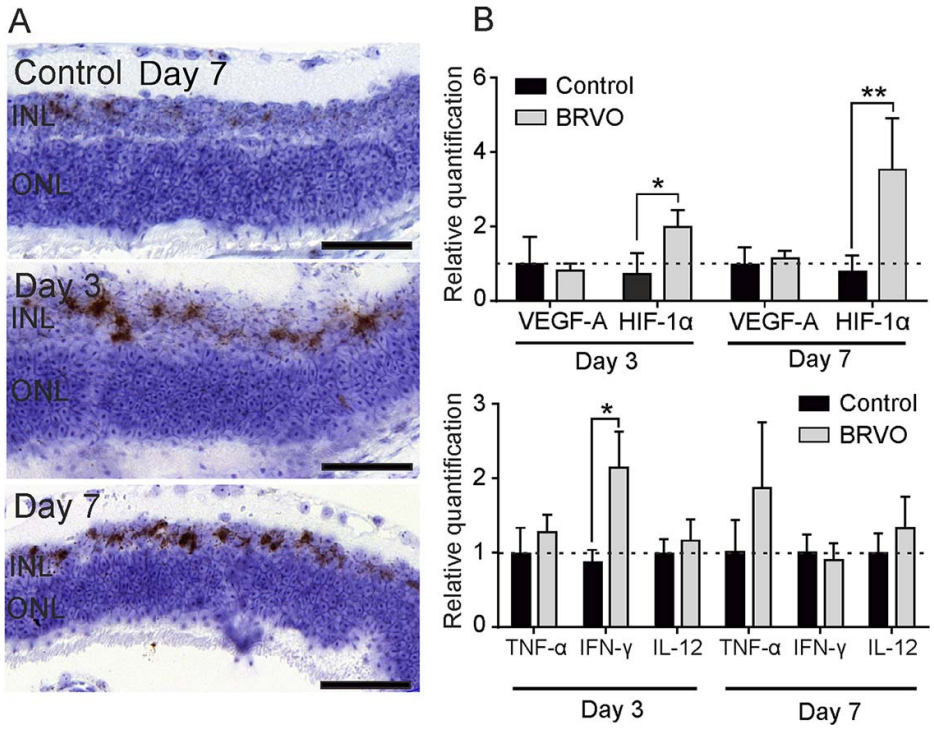

Figure 5. mRNA levels of hypoxia markers and inflammatory cytokines. (**A**) In situ hybridization studies for VEGF mRNA. Elevated levels of VEGF mRNA were detected in the experimental retinas at 3 and 7 days after BRVO. No changes were observed in the control retinas at the different time points. Thus, only one representative picture of control tissue at day 7 is shown. Controls: $n = 3$ at each time point; BRVO: $n = 5$ at each time point. *Scale bars*: 50 μm. INL, inner nuclear layer; ONL, outer nuclear layer. (**B**) Relative quantification of mRNA levels of hypoxia markers and proinflammatory cytokines at 3 and 7 days after BRVO in quantitative real-time PCR. HIF-1α mRNA expression is increased at 3 and 7 days after experimental BRVO ($^*P < 0.05$ and $^{**}P < 0.01$; 2-way ANOVA with post hoc Bonferroni test). The mRNA level of the proinflammatory cytokine IFN-γ was also elevated at day 3 ($^*P < 0.05$; 2-way ANOVA with post hoc Bonferroni test). *Dashed lines* indicate the reference levels (100%), which correspond to naïve retinas. Controls, $n = 5$; BRVO, $n = 8$.

inflammatory processes in the ischemic retina,[4] normally sequestered from the systemic immune system by the blood–ocular barrier.[26] This study confirms that there is a considerable influx of activated bone marrow–derived macrophages, presumably entering mainly through the central retinal artery and optic nerve. Activation was paralleled by significant MHC-II expression in the retina.

Some aspects of our results are comparable to the findings published by Eter et al.[20] in a retina laser lesion model, which primarily disrupts the outer retinal barrier. Similarly, the macrophages remained in the retina for more than 4 weeks. However, in our BRVO model the invasion of macrophages, despite being prompt after the insult, peaked on day 7, somewhat later than in the laser model mentioned before, where the maximum influx was noted around day 2 with ensuing gradual decline. This may reflect a more insidious but longer-lasting disruption of primarily the inner blood–retina barrier. We assume that the major trigger for barrier breakdown in this RVO model is retinal ischemia,[4] which we have shown to be clearly present (Fig. 4), resulting in increased VEGF expression (Fig. 5).

Interestingly, the cells most affected by hypoxia seem to be the Müller cells (Fig. 3), which constitute an important component of the inner blood–retina barrier.[4,27] Increased levels of VEGF mRNA were detected in the inner nuclear layer, a localization consistent with Müller cells, which have been shown previously to express VEGF after hypoxia.[28] Given the central role of this cell type in maintaining homeostasis,[29,30] one can guess the impact of an ischemic insult in the inner retina on the function of the neuroretina. However, in this paradigm, blood–retina barrier disruption and dysfunction seem for the most part not immediate, unlike what is seen in suprathreshold thermal laser injury.[31]

In the retina, microglia are the resident immunocompetent cells, important in triggering inflammatory processes, which can entail invasion of monocyte-derived cells from the systemic circulation.[26,32] Yet activated retinal microglia and blood-derived macrophages express a very similar set of antigens.[33,34] Therefore, the distinction between resident microglia and infiltrating macrophages is not trivial. Chimeric mice using Cx3cr1$^{(gfp/gfp)}$ lines for bone marrow reconstitution after lethal irradiation have proven very useful for this purpose.[33,35,36] It has been shown that repopulation and microglia turnover are normally slow, although differences exist between strains and protocols.[35–39] In the investigated model of BRVO here, invasion of blood-derived macrophages was marked. The main sites of entry were the juxtapapillary region, consistent with the normal path of repopulation in nonlasered chimera, but even more importantly the site of the laser burn and the induced thrombus, where the microglia/macrophages accumulated around the vessel wall like a scar (Fig. 2). The cell morphology patterns observed on Iba-1 whole mounts of wild-type (Fig. 2A) and chimera mice after experimental BRVO (Supplementary Fig.) suggest that the infiltrating cells migrate from the inner retina toward the photoreceptor layer, and while doing so change their morphology from amoeboid to ramified. This hypothesis is also supported observations made by Kezic and McManamin.[36]

Retinal microglia express several surface molecules involved in immune regulation.[40] While major histocompatibility class I molecules and the complement receptor 3 (CR3) are always present but further upregulated in disease, MHC-II

antigens are exclusively expressed by activated micoglia.[23,28,41] We used multichannel FACS with antibodies directed against CD45, CD11b, and CD68 to label highly activated microglia/macrophages. CD68 (macrosialin) is a macrophage-restricted glycoprotein and an accepted marker for phagocytotic activity.[42] Notably, it is often used to label the M2 debris clearing state.[43] In this study, only a minority of these microglia/macrophages (<10%) also expressed MHC-II, required for antigen presentation and T-helper cell interaction. Presumably, phagocytosis of cellular debris occurs in an effort to restore tissue homeostasis by clearing necrotic cells, and consequently to attenuate the detrimental effects of inflammation and aid in tissue repair after irreversible damage.

The model has some inherent weaknesses, such as collateral thermal damage, because laser application disrupts the ocular privilege.[44] However, the risk of damage to the retinal pigment epithelium was limited by choosing albino mice. Furthermore, unspecific laser controls with laser application away from retinal blood vessels were used for comparison. Moreover, eyes were not shielded for lethal irradiation of recipient chimera mice. Irradiation of the retina may itself increase the invasion of donor monocyte-derived cells into the retina.[45]

In summary, this study characterized microglia and macrophage activity in a paradigm that produces predominantly inner retinal hypoxia and subsequently inner blood–retina barrier breakdown. In contrast to models with direct thermal laser damage, the onset of macrophage activity was somewhat delayed, but fundamentally displayed a similar kinetics profile. Only a minority of macrophages expressed MHC-II molecules. Hypoxia markers were predominantly found in Müller cells, which have a critical role in maintaining the integrity of the inner blood–retina barrier. The inflammatory sequelae subsequent to RVO seem substantial, and microglia/macrophages likely play an important role.

Acknowledgments

The authors thank the Department for Clinical Research (DCR) of the University of Bern for the facilities and scientific and technical assistance, and Joel Jovanovic for expert technical assistance. Homozygous fractalkine receptor reporter mice Cx3cr1$^{(gfp/gfp)}$ were generously donated by Steffen Jung (Weizmann Institute of Science, Rehovot, Israel).

Supported by grants from the Inselspital Bern, OPOS foundation and from the Swiss National Science Foundation (Grant# 320030_156019). The sponsor or funding organizations had no role in the design or conduct of the experiments. The authors alone are responsible for the content and writing of this paper.

Disclosure: **A. Ebneter**, Allergan (C, R), Bayer (R), Novartis (R, F), Plexxikon, Inc. (F); **D. Kokona**, Bayer (F); **N. Schneider**, None; **M.S. Zinkernagel**, Bayer (F, C), Heidelberg Engineering (S), Novartis (C, I)

References

1. Rogers S, McIntosh RL, Cheung N, et al. The prevalence of retinal vein occlusion: pooled data from population studies from the United States, Europe, Asia, and Australia. *Ophthalmology*. 2010;117:313–319, e311.
2. Noma H, Funatsu H, Mimura T, Harino S, Hori S. Vitreous levels of interleukin-6 and vascular endothelial growth factor in macular edema with central retinal vein occlusion. *Ophthalmology*. 2009;116:87–93.
3. Noma H, Funatsu H, Mimura T, Tatsugawa M, Shimada K, Eguchi S. Vitreous inflammatory factors and serous macular detachment in branch retinal vein occlusion. *Retina*. 2012;32:86–91.
4. Kaur C, Foulds WS, Ling EA. Blood-retinal barrier in hypoxic ischaemic conditions: basic concepts, clinical features and management. *Prog Retin Eye Res*. 2008;27:622–647.
5. Ehlken C, Grundel B, Michels D, et al. Increased expression of angiogenic and inflammatory proteins in the vitreous of patients with ischemic central retinal vein occlusion. *PLoS One*. 2015;10:e0126859.
6. Noma H, Mimura T, Eguchi S. Association of inflammatory factors with macular edema in branch retinal vein occlusion. *JAMA Ophthalmol*. 2013;131:160–165.
7. Suzuki Y, Nakazawa M, Suzuki K, Yamazaki H, Miyagawa Y. Expression profiles of cytokines and chemokines in vitreous fluid in diabetic retinopathy and central retinal vein occlusion. *Jpn J Ophthalmol*. 2011;55:256–263.
8. Feng J, Zhao T, Zhang Y, Ma Y, Jiang Y. Differences in aqueous concentrations of cytokines in macular edema secondary to branch and central retinal vein occlusion. *PLoS One*. 2013;8:e68149.
9. Noma H, Mimura T, Masahara H, Shimada K. Pentraxin 3 and other inflammatory factors in central retinal vein occlusion and macular edema. *Retina*. 2014;34:352–359.
10. O'Koren EG, Mathew R, Saban DR. Fate mapping reveals that microglia and recruited monocyte-derived macrophages are definitively distinguishable by phenotype in the retina. *Sci Rep*. 2016;6:20636.
11. Karlstetter M, Scholz R, Rutar M, Wong WT, Provis JM, Langmann T. Retinal microglia: just bystander or target for therapy? *Prog Retin Eye Res*. 2015;45:30–57.
12. Mantovani A, Sica A, Sozzani S, Allavena P, Vecchi A, Locati M. The chemokine system in diverse forms of macrophage activation and polarization. *Trends Immunol*. 2004;25:677–686.
13. Scott IU, Ip MS, VanVeldhuisen PC, et al. A randomized trial comparing the efficacy and safety of intravitreal triamcinolone with standard care to treat vision loss associated with macular edema secondary to branch retinal vein occlusion: the Standard Care vs Corticosteroid for Retinal Vein Occlusion (SCORE) study report 6. *Arch Ophthalmol*. 2009;127:1115–1128.
14. Ding X, Li J, Hu X, Yu S, Pan J, Tang S. Prospective study of intravitreal triamcinolone acetonide versus bevacizumab for macular edema secondary to central retinal vein occlusion. *Retina*. 2011;31:838–845.
15. Clark WL, Boyer DS, Heier JS, et al. Intravitreal aflibercept for macular edema following branch retinal vein occlusion: 52-week results of the VIBRANT Study. *Ophthalmology*. 2016;123:330–336.
16. Heier JS, Campochiaro PA, Yau L, et al. Ranibizumab for macular edema due to retinal vein occlusions: long-term follow-up in the HORIZON trial. *Ophthalmology*. 2012;119:802–809.
17. Korobelnik JF, Holz FG, Roider J, et al. Intravitreal aflibercept injection for macular edema resulting from central retinal vein occlusion: one-year results of the phase 3 GALILEO Study. *Ophthalmology*. 2014;121:202–208.
18. Rutar M, Provis JM. Role of chemokines in shaping macrophage activity in AMD. *Adv Exp Med Biol*. 2016;854:11–16.
19. Grunin M, Hagbi-Levi S, Chowers I. The role of monocytes and macrophages in age-related macular degeneration. *Adv Exp Med Biol*. 2014;801:199–205.
20. Eter N, Engel DR, Meyer L, et al. In vivo visualization of dendritic cells, macrophages, and microglial cells responding to laser-induced damage in the fundus of the eye. *Invest Ophthalmol Vis Sci*. 2008;49:3649–3658.
21. Ebneter A, Agca C, Dysli C, Zinkernagel MS. Investigation of retinal morphology alterations using spectral domain optical coherence tomography in a mouse model of retinal branch

and central retinal vein occlusion. *PLoS One*. 2015;10: e0119046.

22. Dominguez E, Raoul W, Calippe B, et al. Experimental branch retinal vein occlusion induces upstream pericyte loss and vascular destabilization. *PLoS One*. 2015;10:e0132644.
23. Ebneter A, Casson RJ, Wood JP, Chidlow G. Microglial activation in the visual pathway in experimental glaucoma: spatiotemporal characterization and correlation with axonal injury. *Invest Ophthalmol Vis Sci*. 2010;51:6448–6460.
24. Kuonen F, Touvrey C, Laurent J, Ruegg C. Fc block treatment, dead cells exclusion, and cell aggregates discrimination concur to prevent phenotypical artifacts in the analysis of subpopulations of tumor-infiltrating CD11b(+) myelomonocytic cells. *Cytometry A*. 2010;77:1082–1090.
25. del Zoppo GJ. Acute anti-inflammatory approaches to ischemic stroke. *Ann N Y Acad Sci U S A*. 2010;1207:143–148.
26. Forrester JV, Xu H, Kuffova L, Dick AD, McMenamin PG. Dendritic cell physiology and function in the eye. *Immunol Rev*. 2010;234:282–304.
27. Tretiach M, Madigan MC, Wen L, Gillies MC. Effect of Müller cell co-culture on in vitro permeability of bovine retinal vascular endothelium in normoxic and hypoxic conditions. *Neurosci Lett*. 2005;378:160–165.
28. Kaur C, Sivakumar V, Foulds WS. Early response of neurons and glial cells to hypoxia in the retina. *Invest Ophthalmol Vis Sci*. 2006;47:1126–1141.
29. Bringmann A, Pannicke T, Grosche J, et al. Müller cells in the healthy and diseased retina. *Prog Retin Eye Res*. 2006;25:397–424.
30. Reichenbach A, Bringmann A. New functions of Müller cells. *Glia*. 2013;61:651–678.
31. Jain A, Blumenkranz MS, Paulus Y, et al. Effect of pulse duration on size and character of the lesion in retinal photocoagulation. *Arch Ophthalmol*. 2008;126:78–85.
32. Karlstetter M, Ebert S, Langmann T. Microglia in the healthy and degenerating retina: insights from novel mouse models. *Immunobiology*. 2010;215:685–691.
33. Kezic J, McMenamin PG. The monocyte chemokine receptor CX3CR1 does not play a significant role in the pathogenesis of experimental autoimmune uveoretinitis. *Invest Ophthalmol Vis Sci*. 2010;51:5121–5127.
34. Ulvestad E, Williams K, Bjerkvig R, Tiekotter K, Antel J, Matre R. Human microglial cells have phenotypic and functional characteristics in common with both macrophages and dendritic antigen-presenting cells. *J Leukoc Biol*. 1994;56: 732–740.
35. Kezic JM, McMenamin PG. The effects of CX3CR1 deficiency and irradiation on the homing of monocyte-derived cell populations in the mouse eye. *PLoS One*. 2013;8:e68570.
36. Kezic J, McMenamin PG. Differential turnover rates of monocyte-derived cells in varied ocular tissue microenvironments. *J Leukoc Biol*. 2008;84:721–729.
37. Xu H, Chen M, Mayer EJ, Forrester JV, Dick AD. Turnover of resident retinal microglia in the normal adult mouse. *Glia*. 2007;55:1189–1198.
38. Kaneko H, Nishiguchi KM, Nakamura M, Kachi S, Terasaki H. Characteristics of bone marrow-derived microglia in the normal and injured retina. *Invest Ophthalmol Vis Sci*. 2008; 49:4162–4168.
39. Albini TA, Wang RC, Reiser B, Zamir E, Wu GS, Rao NA. Microglial stability and repopulation in the retina. *Br J Ophthalmol*. 2005;89:901–903.
40. Chen L, Yang P, Kijlstra A. Distribution, markers, and functions of retinal microglia. *Ocul Immunol Inflamm*. 2002;10:27–39.
41. Zhang C, Lam TT, Tso MO. Heterogeneous populations of microglia/macrophages in the retina and their activation after retinal ischemia and reperfusion injury. *Exp Eye Res*. 2005;81: 700–709.
42. Holness CL, da Silva RP, Fawcett J, Gordon S, Simmons DL. Macrosialin, a mouse macrophage-restricted glycoprotein, is a member of the lamp/lgp family. *J Biol Chem*. 1993;268:9661–9666.
43. Perego C, Fumagalli S, De Simoni MG. Temporal pattern of expression and colocalization of microglia/macrophage phenotype markers following brain ischemic injury in mice. *J Neuroinflammation*. 2011;8:174.
44. Qiao H, Lucas K, Stein-Streilein J. Retinal laser burn disrupts immune privilege in the eye. *Am J Pathol*. 2009;174:414–422.
45. Ajami B, Bennett JL, Krieger C, Tetzlaff W, Rossi FM. Local self-renewal can sustain CNS microglia maintenance and function throughout adult life. *Nat Neurosci*. 2007;10:1538–1543.

Investigative Ophthalmology & Visual Science